The Astrophysical Journal Letters, 848:L20 (7pp), 2017 October 20 https://doi.org/10.3847/2041-8213/aa9057
© 2017. The American Astronomical Society. All rights reserved.

The Electromagnetic Counterpart of the Binary Neutron Star Merger LIGO/Virgo GW170817. V. Rising X-Ray Emission from an Off-axis Jet

R. Margutti[1], E. Berger[2], W. Fong[1,13], C. Guidorzi[3], K. D. Alexander[2], B. D. Metzger[4], P. K. Blanchard[2], P. S. Cowperthwaite[2], R. Chornock[5], T. Eftekhari[2], M. Nicholl[2], V. A. Villar[2], P. K. G. Williams[2], J. Annis[6], D. A. Brown[7], H. Chen[8], Z. Doctor[8], J. A. Frieman[6,9], D. E. Holz[9,10], M. Sako[11], and M. Soares-Santos[6,12]

[1] Center for Interdisciplinary Exploration and Research in Astrophysics (CIERA) and Department of Physics and Astronomy, Northwestern University, Evanston, IL 60208, USA
[2] Harvard-Smithsonian Center for Astrophysics, 60 Garden Street, Cambridge, MA 02138, USA
[3] Department of Physics and Earth Science, University of Ferrara, via Saragat 1, I-44122, Ferrara, Italy
[4] Department of Physics and Columbia Astrophysics Laboratory, Columbia University, New York, NY 10027, USA
[5] Astrophysical Institute, Department of Physics and Astronomy, 251B Clippinger Lab, Ohio University, Athens, OH 45701, USA
[6] Fermi National Accelerator Laboratory, P.O. Box 500, Batavia, IL 60510, USA
[7] Physics Department, Syracuse University, Syracuse, NY 13244, USA
[8] Department of Astronomy and Astrophysics, University of Chicago, Chicago, IL 60637, USA
[9] Kavli Institute for Cosmological Physics, University of Chicago, Chicago, IL 60637, USA
[10] Enrico Fermi Institute, Department of Physics, Department of Astronomy and Astrophysics, University of Chicago, Chicago, IL 60637, USA
[11] Department of Physics and Astronomy, University of Pennsylvania, Philadelphia, PA 19104, USA
[12] Department of Physics, Brandeis University, Waltham, MA 02454, USA
Received 2017 September 27; revised 2017 September 29; accepted 2017 September 30; published 2017 October 16

Abstract

We report the discovery of rising X-ray emission from the binary neutron star merger event GW170817. This is the first detection of X-ray emission from a gravitational-wave (GW) source. Observations acquired with the *Chandra X-ray Observatory* (*CXO*) at $t \approx 2.3$ days post-merger reveal no significant emission, with $L_x \lesssim 3.2 \times 10^{38}$ erg s^{-1} (isotropic-equivalent). Continued monitoring revealed the presence of an X-ray source that brightened with time, reaching $L_x \approx 9 \times 10^{38}$ erg s^{-1} at $\approx$15.1 days post-merger. We interpret these findings in the context of isotropic and collimated relativistic outflows (both on- and off-axis). We find that the broadband X-ray to radio observations are consistent with emission from a relativistic jet with kinetic energy $E_k \sim 10^{49-50}$ erg, viewed off-axis with $\theta_{\rm obs} \sim 20°$–$40°$. Our models favor a circumbinary density $n \sim 10^{-4}$–10^{-2} cm^{-3}, depending on the value of the microphysical parameter $\epsilon_B = 10^{-4}$–10^{-2}. A central-engine origin of the X-ray emission is unlikely. Future X-ray observations at $t \gtrsim 100$ days, when the target will be observable again with the *CXO*, will provide additional constraints to solve the model degeneracies and test our predictions. Our inferences on $\theta_{\rm obs}$ are testable with GW information on GW170817 from advanced LIGO/Virgo on the binary inclination.

Key words: stars: neutron – gravitational waves – relativistic processes

1. Introduction

Gravitational waves (GWs) from the merger of a binary neutron star (BNS) system were detected for the first time by advanced LIGO and advanced Virgo on 2017 August 17.53 UT (Abbott et al. 2017; LIGO Scientific Collaboration & Virgo Collaboration 2017a). The GW event, named GW170817, was localized to a region of $\sim$30 deg^2 with a distance of $\sim$40 Mpc. The GW signal from the BNS merger was closely followed in time by a short burst of γ-ray emission detected by *Fermi* and *INTEGRAL* (Connaughton et al. 2017; Savchenko et al. 2017) with fluence $F_\gamma = (2.4 \pm 0.5) \times 10^{-7}$ erg cm^{-2} (Goldstein et al. 2017). These observations established GW170817 to be the first astrophysical event with GW and EM detections, marking the dawn of multi-messenger astrophysics.[14]

Optical observations acquired within $\sim$12 hr after the GW detection led to the discovery and localization of a transient with peculiar properties in the outskirts of the galaxy NGC 4993 (Allam et al. 2017; Blanchard et al. 2017; Coulter et al. 2017b; Soares-Santos et al. 2017; Valenti et al. 2017; Yang et al. 2017); see Soares-Santos et al. (2017) for details of our group's discovery. Intense photometric and spectroscopic UV/optical/NIR monitoring of the transient (Chornock et al. 2017; Cowperthwaite et al. 2017; Nicholl et al. 2017) revealed an evolution that closely follows the theoretical expectations from a "kilonova," i.e., a transient powered by the radioactive decay of *r*-process nuclei synthesized in the neutron-rich merger ejecta (see Metzger 2017 for a recent review).

Non-thermal radiation at X-ray and radio wavelengths is also expected to be associated with BNS mergers on different timescales and luminosities *if* these systems are able to launch relativistic jets, as initially postulated in the case of short gamma-ray bursts (SGRBs; e.g., Eichler et al. 1989; Narayan et al. 1992). Observations of the environments and properties of emission of SGRBs in the past decade provided solid indirect evidence of the association of SGRBs with BNS mergers (Fong & Berger 2013; Berger 2014; Fong et al. 2015), thus motivating our search for observational signatures of on-axis and off-axis jets in GW170817.

Here, we report the first detection of X-ray emission from a GW event. We explore various scenarios for the origin of the

[13] Hubble Fellow.
[14] Note that the optical transient source was given the name of SSS17a (Coulter et al. 2017a, 2017b) and DLT17ck (Valenti et al. 2017; Yang et al. 2017), as well as an the IAU name of AT2017gfo.

X-ray emission and place constraints on the properties of the circumbinary medium, jet energetics, collimation, and observer angle based on the broadband X-ray to radio observations. A comparison to the properties of "canonical" SGRBs can be found in Fong et al. (2017a), while we refer to our companion paper Alexander et al. (2017a) for a dedicated discussion of the radio observations of GW170817. Our X-ray observations of NGC 4993, the host galaxy of GW170817, are discussed in Blanchard et al. (2017).

We assume a distance to NGC 4993 of 39.5 Mpc ($z = 0.00973$) as listed in the NASA Extragalactic Database. 1σ c.l. uncertainties are listed unless otherwise stated. In this Letter, we employ the notation $Q_x \equiv Q/10^x$. In this paper we always refer to isotropic-equivalent luminosities. We differentiate between isotropic-equivalent kinetic energy $E_{k,\rm iso}$, and beaming-corrected kinetic energy of the blast wave E_k, where $E_k = E_{k,\rm iso}(1 - \cos(\theta_j))$ and θ_j is the jet opening angle.

2. Observations

With the Dark Energy Camera, we independently discovered and localized the optical transient to R.A. = $13^{\rm h}09^{\rm m}48\overset{\rm s}{.}08$, decl. = $-23°22'53\overset{''}{.}2$ (J2000) with 1σ uncertainties of 130 mas and 60 mas, respectively (Soares-Santos et al. 2017), and initiated multi-wavelength follow-up of the transient across the electromagnetic spectrum. Here, we report on X-ray observations that led to the first identification of rising X-ray emission from a BNS merger event GW170817.

2.1. Swift X-Ray Observations

The *Swift* spacecraft (Gehrels et al. 2004) started observations of the optical counterpart of LIGO/Virgo GW170817 (Allam et al. 2017; Coulter et al. 2017a, 2017b; Soares-Santos et al. 2017; Yang et al. 2017) with the X-ray telescope (XRT; Burrows et al. 2005) on August 18, 03:33:33UT, 14.9 hr after the GW trigger. *Swift*-XRT observations span the time range 0.6–11.5 days since trigger, at which point the target entered into Sun constraint. *Swift*-XRT data have been analyzed using HEASOFT (v6.22) and corresponding calibration files, employing standard filtering criteria and following standard procedures (see Margutti et al. 2013 for details). No transient X-ray emission is detected at the location of the GW optical counterpart (Cenko et al. 2017; Evans et al. 2017a, 2017b), with typical count-rate limits of $\sim$ a few 10^{-3} c s^{-1}. The neutral hydrogen column density in the direction of the transient is $\rm NH_{\it mw} = 0.0784 \times 10^{22}$ cm^{-2} (Kalberla et al. 2005). For a typical absorbed power-law spectrum with photon index $\Gamma \sim 2$ and negligible intrinsic absorption (see below), the corresponding 3σ flux limit is $\sim 10^{-13}$ erg s^{-1} cm^{-2} (unabsorbed, 0.3–10 keV), which is $L_x <$ a few 10^{40} erg s^{-1} at the distance of 39.5 Mpc. As we show in detail in Fong et al. (2017a), *Swift*-XRT observations constrain the X-ray emission associated with the optical counterpart of LIGO/Virgo GW170817 to be significantly fainter than cosmological short GRBs at the same epoch (Margutti et al. 2013; D'Avanzo et al. 2014; Fong et al. 2015).

2.2. Chandra X-Ray Observations

We initiated deep X-ray follow-up of the optical transient with the *Chandra X-ray Observatory* (*CXO*) on 2017 August 19.71 UT, $\delta t \approx 2.3$ d after the GW detection (observation ID 18955; PI: Fong; Program 18400052). *Chandra* ACIS-S data have been reduced with the `CIAO` software package (v4.9) and relative calibration files, applying standard ACIS data filtering. Using `wavdetect` we find no evidence for X-ray emission at the position of the optical transient (Margutti et al. 2017) and we infer a 3σ limit of 1.2×10^{-4}cps (0.5–8 keV energy range, total exposure time of 24.6 ks). For an assumed absorbed spectral power-law model with $\Gamma = 2$, negligible intrinsic absorption, and $\rm NH_{\it mw} = 0.0784 \times 10^{22}$ cm^{-2}, the corresponding absorbed (unabsorbed) flux limit in the 0.3–10 keV energy range is $F_{\rm x} < 1.4 \times 10^{-15}$ erg s^{-1} cm^{-2} ($F_{\rm x} < 1.7 \times 10^{-15}$ erg s^{-1} cm^{-2}).[15] The luminosity limit is $L_{\rm x} < 3.2 \times 10^{38}$ erg s^{-1} (0.3–10 keV), making the X-ray counterpart to GW170817 $\geqslant 1000$ times fainter than on-axis short GRBs at the same epoch (Fong et al. 2017a).

We re-visited the location of the optical transient on September 1.64 UT (starting 15.1 days since the trigger) under a DDT program with shared data (observation ID 20728; data shared among Troja, Haggard, and Margutti; Program 18508587; official PI: Troja) with an effective exposure time of 46.7 ks. An X-ray source is blindly detected (Fong et al. 2017b) with high significance of $\sim 7.3\sigma$ at R.A. = $13^{\rm h}09^{\rm m}48\overset{\rm s}{.}076$ and decl. = $-23°22'53\overset{''}{.}34$ (J2000), see Figure 1, consistent with the optical transient and the findings by Troja et al. (2017a, 2017b).

The source 0.5–8 keV count rate is $(3.8 \pm 0.9) \times 10^{-4}$ cps. The total number of 0.5–8 keV counts in the source region is 19. Based on Poissonian statistics, the probability to observe 0 events in 24.6 ks (as in our first observation), if the expected rate is 19 events in 46.7 ks, is $\sim$0.0045% ($\sim$4 Gaussian σ equivalent). A similar result is obtained with a Binomial test ($P \sim 0.03\%$, corresponding to $\sim$3.6 Gaussian σ). *We can thus reject the hypothesis of a random fluctuation of a persistent X-ray source with high confidence, and we conclude that we detected rising X-ray emission in association with the optical counterpart to GW170817.*

The limited statistics does not allow us to constrain the spectral model. We employ Cash statistics to fit the spectrum with an absorbed power-law spectral model with index Γ and perform a series of Markov Chain Monte Carlo simulations to constrain the spectral parameters. We find $\Gamma = 1.6^{+1.5}_{-0.1}$ (1σ c.l.) with no evidence for intrinsic neutral hydrogen absorption $\rm NH_{int} < 3 \times 10^{22}$ cm^{-2} (3σ c.l.). For these parameters, the inferred 0.3–10 keV flux is $(3.0–5.6) \times 10^{-15}$ erg s^{-1} cm^{-2} (1σ c.l.). The corresponding unabsorbed flux is $(3.1–5.8) \times 10^{-15}$ erg s^{-1} cm^{-2}, and luminosity L_x is in the range $(5.9–11.1) \times 10^{38}$ erg s^{-1} (1σ c.l.).

Figure 2 shows our *CXO* light curve of the X-ray source associated with GW170817. In this figure, we add the X-ray measurement by Haggard et al. (2017a, 2017b) obtained 15.9 days after GW trigger (PI: Haggard, ID 18988) and rescaled to $\Gamma = 2$ in the 0.3–10 keV energy range, leading to $F_x \sim 4.5 \times 10^{-15}$ erg s^{-1} cm^{-2}. This flux is consistent with

[15] Significant intrinsic absorption is not expected, given the early-type nature of the host galaxy and the location of the transient in the outskirts of its host galaxy (Blanchard et al. 2017). This expectation is independently confirmed by our optical/NIR modeling (Blanchard et al. 2017), which indicates $\rm NH_{int} < 10^{21}$ cm^{-2}, and by the X-ray analysis of the epoch when the transient is detected. However, we repeated our analysis of the first *CXO* epoch focusing on the harder part of the spectrum to minimize the possible effects of absorption. We find a 3σ limit of 1.2×10^{-4} cps (0.8–8 keV), which corresponds to a limit on the flux density at 1 keV $F_{\rm 1\,keV} < 1.40 \times 10^{-4}$ μJy. With the previous spectral calibration we would infer a similar value $F_{\rm 1\,keV} < 1.32 \times 10^{-4}$ μJy. We conclude that our modeling below, which employs $F_{\rm 1\,keV}$ is thus robust.

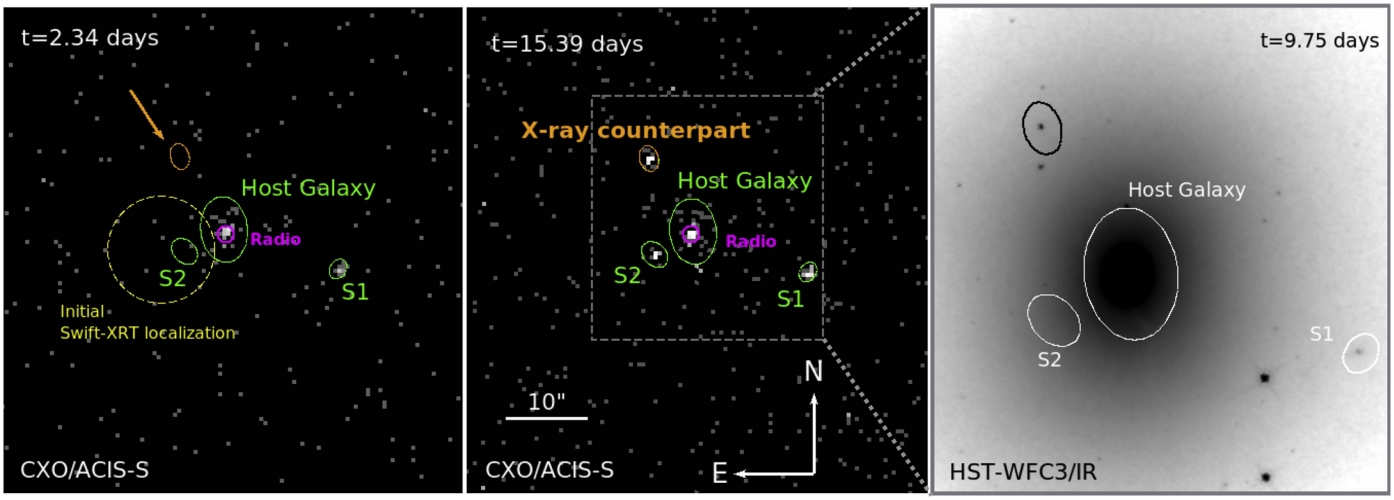

Figure 1. 0.5–8 keV *CXO* observations of the optical transient associated with GW170817 obtained at ∼2.34 days (left panel) and ∼15.39 days (central panel) since BNS coalescence revealed the appearance of a new X-ray source at the location of the optical transient (right panel). The host galaxy is a source of diffuse and persistent X-ray emission, with the core of the X-ray emission coincident with the radio source (1″ magenta region) that we identified in Alexander et al. (2017b), suggesting the presence of a weak AGN (Blanchard et al. 2017). The central panel also shows the appearance of another X-ray source, S2, which was not detected in our first *CXO* observations. The initial localization of an X-ray source by the *Swift*-XRT at $t < 2$ days (Evans et al. 2017b; yellow dashed region in the left panel, 90% containment) might suggest that S2 was "active" before our first *CXO* observation. Right panel: zoom-in into *HST* observations of the EM counterpart to GW170817 (Blanchard et al. 2017; Nicholl et al. 2017) with the X-ray regions overlaid.

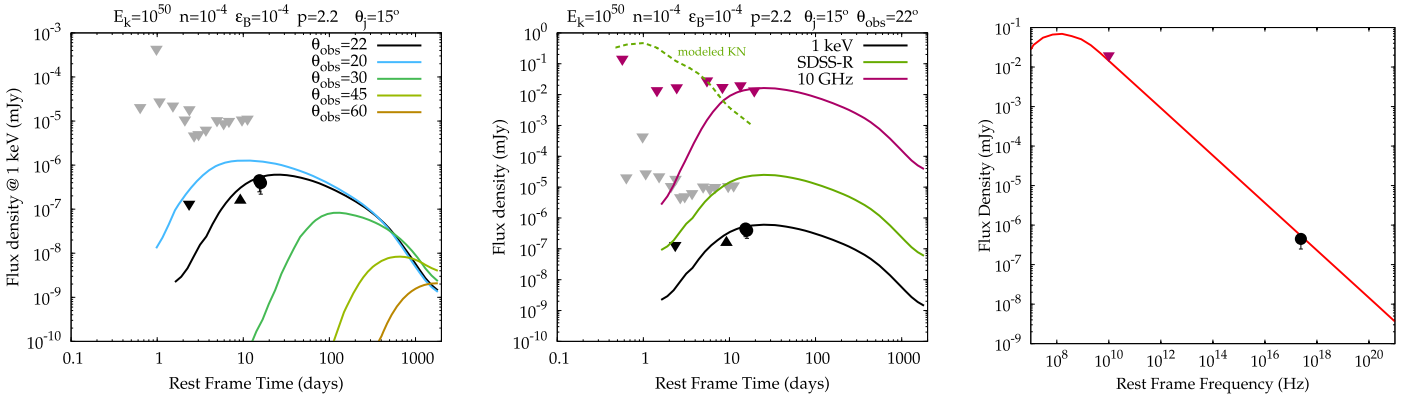

Figure 2. Off-axis jet model with $\theta_j = 15°$ and $E_k = 10^{50}$ erg that best represents the current set of X-ray and radio observations (see Figure 3 for models with $E_k = 10^{49}$ erg). For this model, $n = 10^{-4}$ cm^{-3}, $\epsilon_B = 10^{-4}$. Left panel: X-ray emission for observers at different θ_{obs} (colored lines). The black line identifies the best-fitting model, which has $\theta_{obs} \sim 22°$. Gray triangles: *Swift*-XRT upper limits. Black symbols: *CXO* observations. We show the results from Troja et al. (2017a, 2017b) as an upward triangle (lower limit) for graphics purposes only. Central panel: radio (10 GHz; solid purple line) and optical emission (r-band; solid green line) for the best-fitting model compared to our VLA limits (purple triangles; Alexander et al. 2017a) and emission from the kilonova (green dashed line; Cowperthwaite et al. 2017). The optical off-axis afterglow represents a negligible contribution to the kilonova emission at $t < 30$ days. Right column: SED of the best-fitting model at the time of the X-ray detection 15.4 days. The best-fitting off-axis models with $E_k = 10^{49}$ erg are shown in Figure 3.

our observations obtained ∼24 hr before, with no statistically significant evidence for temporal variability of the source on this timescale. An estimate of the lower limit of the X-ray flux at $t \sim 10$ days, corresponding to the reported detection of X-ray emission with the *CXO* using an exposure time of 50 ks (Troja et al. 2017a, 2017b) is also shown to guide the eye.

3. Origin of the Rising X-Ray Emission

We discuss the physical origin of the rising X-ray emission found in association with GW170817 considering the following observational constraints. (i) The peak of the X-ray emission is at $t_{pk} \geqslant 15$ days. (ii) The X-ray light curve shows mild temporal evolution, with no signs of rise or decay over a ∼24 hr timescale at $t \sim 15$ days. (iii) The blue colors of the early kilonova emission (Cowperthwaite et al. 2017; Nicholl et al. 2017) suggest $\theta_{obs} < 45°$ (Sekiguchi et al. 2016), where θ_{obs} is the observer angle with respect to the jet axis (Section 3.2).[16] (iv) Simultaneous radio observations from Alexander et al. (2017a) that include the earliest radio observations of this transient at different frequencies and detections at 6 GHz. Below, we discuss the nature of the X-ray emission from GW170817 considering this entire range of observational constraints available at the time of writing.

3.1. Constraints on On-axis Outflows

We first consider constraints on on-axis[17] relativistic outflows (collimated or not collimated), under the assumption that the the

[16] As a note of caution, we mention here that it might be possible to observe blue emission from a kilonova even from larger viewing angles if it expands faster than the tidal matter. This scenario has yet to be fully explored.

[17] In other words, outflows for which $\theta_{obs} \leqslant \theta_j$, where θ_j is the half-opening angle of the core of the jet and θ_{obs} is the observer angle with respect to the jet axis.

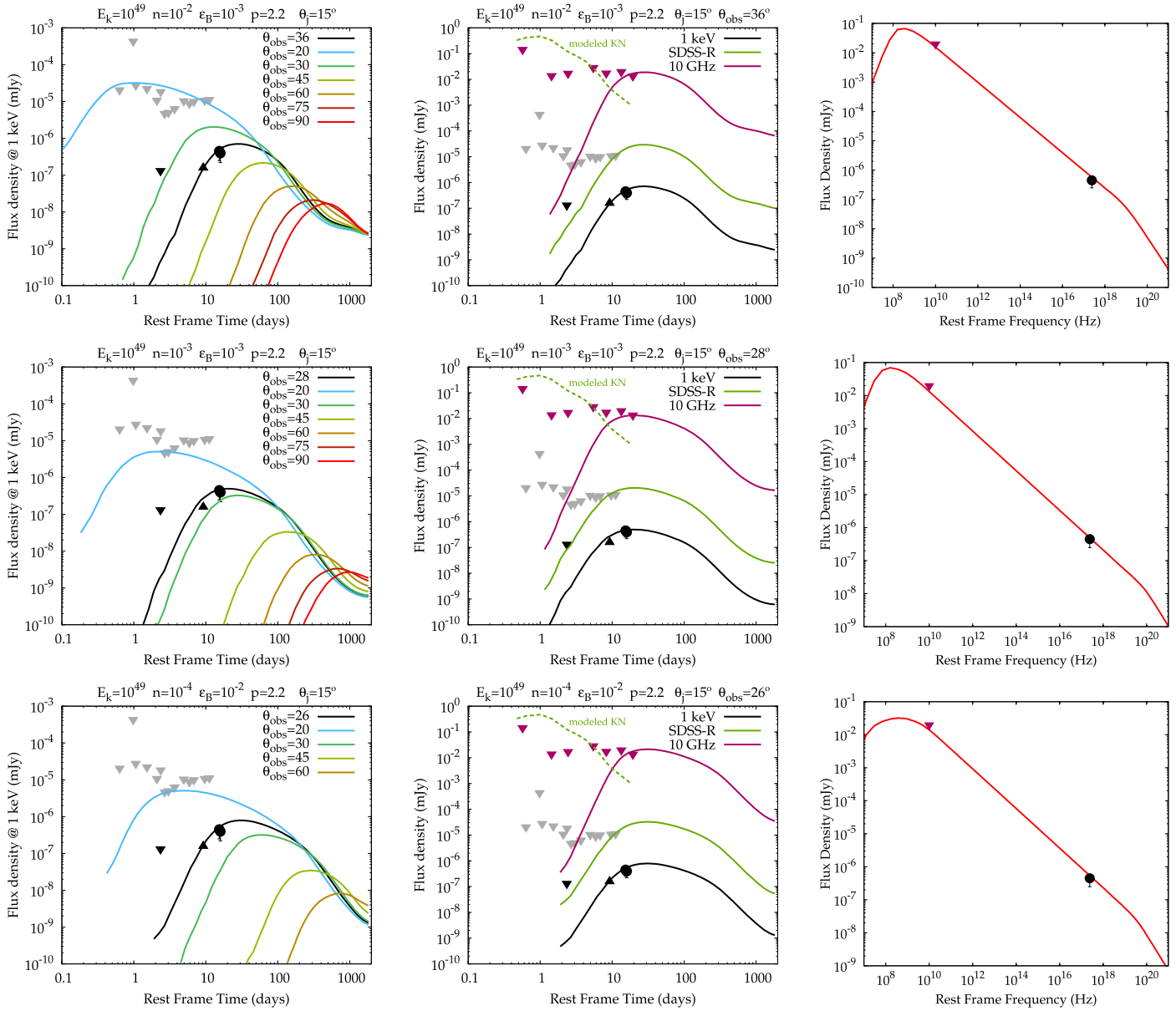

Figure 3. Off-axis jet models with $\theta_j = 15°$ and $E_k = 10^{49}$ erg that best represents the current set of X-ray and radio observations. Each row is dedicated to a jet model with a given set of parameters n, ϵ_B. Color-coding as in Figure 2. Left column: X-ray emission for a jet with parameters indicated in each plot title and for observers at different $\theta_{\rm obs}$ (colored lines). The black line identifies the best-fitting model. Gray triangles: *Swift*-XRT upper limits. Black symbols: *CXO* observations. Central panel: radio (10 GHz; solid purple line) and optical emission (r-band; solid green line) for the best-fitting model compared to our VLA limits (purple triangles; Alexander et al. 2017a) and emission from the kilonova (green dashed line; Cowperthwaite et al. 2017). The optical off-axis afterglow represents a negligible contribution to the kilonova emission at $t < 30$ days. Right column: SED of the best-fitting model at the time of the X-ray detection 15.4 days. The best-fitting off-axis model for $E_k = 10^{50}$ erg is shown in Figure 2.

blast wave has transferred to the interstellar medium (ISM) most of its energy by the time of our first *CXO* observation, and its hydrodynamics is thus well described by the Blandford-McKee (BM) self-similar deceleration solution (Blandford & McKee 1976). Electrons are accelerated at the shock front into a power-law distribution $N(\gamma) \propto \gamma^{-p}$ for $\gamma \geqslant \gamma_{\rm min}$ and cool through synchrotron emission and adiabatic losses.

In the standard synchrotron model (e.g., Granot & Sari 2002), the flux density $F_\nu \propto n^{1/2} E_{k,\rm iso}^{(3+p)/4} \epsilon_e^{p-1} \epsilon_B^{(1+p)/4} t^{(3-3p)/4}$ if the X-rays are on the $\nu^{(1-p)/2}$ spectral segment (i.e., $\nu_x < \nu_c$) and $F_\nu \propto E_{k,\rm iso}^{(2+p)/4} \epsilon_e^{p-1} \epsilon_B^{(p-2)/4} t^{(2-3p)/4}$ if the X-rays are on the $\nu^{-p/2}$ spectral segment ($\nu_x > \nu_c$). ν_c is the synchrotron cooling frequency (e.g., Rybicki & Lightman 1979), ϵ_e and ϵ_B are the post-shock energy fractions in electrons and magnetic field, respectively, and n is the ISM density. We use a constant density medium as expected for a non-massive star progenitor.

Within this model, and for fiducial parameters $\epsilon_e = 0.1$, $\epsilon_B = 0.01$, and $p = 2.4$ set by the median value of cosmological short GRBs (Fong et al. 2015), the deep *CXO* non-detection on day 2.34 constrains $E_{k,\rm iso} \leqslant 10^{47} n_0^{-10/27}$ erg for $\nu_x < \nu_c$ and $E_{k,\rm iso} \leqslant 4 \times 10^{46}$ erg for $\nu_x > \nu_c$. n_0 is the circumburst density in units of cm^{-3}. Consistent with the results from radio observations (Alexander et al. 2017a), this analysis points at low $E_{k,\rm iso} \leqslant 10^{48}$ erg for the range of densities $n \sim$ (3–15) $\times 10^{-3}$ cm^{-3} associated with cosmological short GRBs, which are characterized by

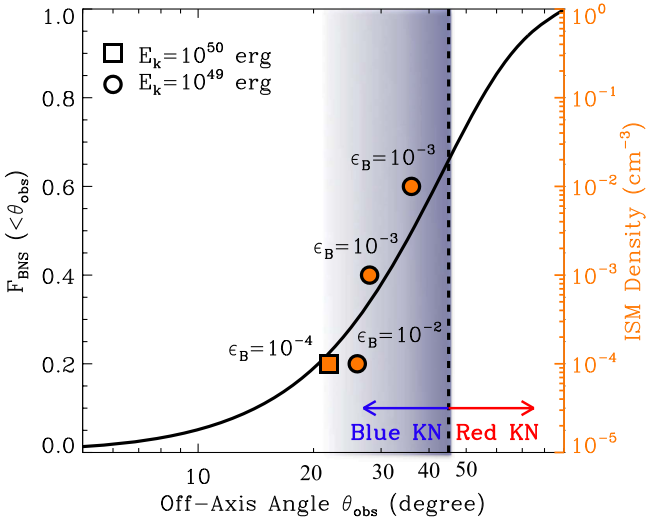

Figure 4. Left y-axis and black thick line: cumulative GW detection probability at observing angles $<\theta_{\rm obs}$ with respect to the binary axis, calculated following Metzger & Berger (2012) and Schutz (2011). Orange points: $\theta_{\rm obs}$ as inferred from our simulations of off-axis jets with $E_k = 10^{49}$ erg (filled circles) or $E_k = 10^{50}$ erg (filled square) and $\theta_j = 15^\circ$ that satisfy all the observational constraints from X-ray and radio observations currently available, as a function of the ISM density n (right y-axis). A kilonova with blue colors is expected for $\theta_{\rm obs} \leqslant 45^\circ$ (Sekiguchi et al. 2016; shaded blue area). The value of ϵ_B for each successful simulation is also reported in the plot.

Table 1
BOXFIT Parameters

Parameter	Values Considered
Jet energy $E_{\rm k}$ (erg)	10^{48}, 10^{49}, 10^{50}, 10^{51}
Circum-merger density n (cm^{-3})	10^{-4}, 10^{-3}, 10^{-2}, 0.1, 1
Jet opening angle $\theta_{\rm j}$ (deg)	5, 15
Observer angle $\theta_{\rm obs}$ (deg)	0, 5, 10, 20, 30, 45, 60, 75, 90
Fraction of post-shock energy in B ϵ_B	10^{-4}, 10^{-3}, 10^{-2}
Power-law index of electron distribution p	2.2, 2.4

Note. Simulations were run at fixed values $\epsilon_e = 0.1$ in a constant density medium.

$E_{k,\rm iso} \sim (1\text{–}3) \times 10^{51}$ erg for the same microphysical parameters $\epsilon_e = 0.1$ and $\epsilon_B = 0.01$ (Fong et al. 2015). We note that this conclusion does not depend on the choice of p, with $p = 2.1\text{–}2.4$ ($p > 2.4$ violates our radio limits). This solution is only valid during the relativistic phase at $t < t_{NR}$ (where $t_{NR} \sim 1100\ (E_{k,\rm iso}/10^{53} n_0)^{1/3}$ days; Piran 2004) and constrains the presence of an undetected, temporally *decaying* X-ray emission at $t < 2.34$ days, with properties that are clearly distinguished from cosmological short GRBs seen on-axis (Fong et al. 2017a).

A *rising* X-ray light curve can be the result of a delayed onset of the afterglow emission, as the blast wave decelerates into the environment and transfers energy to the circumburst medium. In this scenario, the initial Lorentz factor of the outflow is $\Gamma_0 \sim 8.0\, E_{k,\rm iso,52}^{1/8} n_0^{-1/8} t_{\rm pk,day}^{-3/8}$, where $t_{\rm pk,day}$ is the peak time of the afterglow in days (Sari & Piran 1999). A distinguishing feature of the early afterglow emission is an initial very steep rise of the emission $\propto t^2$ or $\propto t^{11/3}$ (Sari & Piran 1999). The stable X-ray flux of the source at $t \sim 15\text{–}16$ days suggests that $t_{\rm pk} \sim 15\text{–}30$ days. Given the *Fermi*-GBM detection of a gamma-ray transient with fluence $F \sim 2.4 \times 10^{-7}$ erg cm^{-2} (Goldstein et al. 2017), which gives $E_{k,\rm iso} \sim 5 \times 10^{47}$ erg for a fiducial γ-ray efficiency $\eta_\gamma = 0.1$, we infer a mildly relativistic $\Gamma_0 \sim 2$ for $t_{\rm pk} \sim 15\text{–}30$ days. After peak, when most of the fireball energy has been transferred to the ISM, the standard afterglow scalings apply. The latest *CXO* detection implies $E_{k,\rm iso} \sim 10^{48} n_0^{-10/27}$ erg if $\nu_x < \nu_c$, or $E_{k,\rm iso} \sim 10^{48}$ erg for $\nu_x > \nu_c$. Radio observations acquired around the same time (Alexander et al. 2017a) constrain $p \approx 2.2$. Mildly relativistic outflows with similar Γ and E_k that are found in shocks from supernovae (SN) with fast ejecta (i.e., relativistic SNe) are well described by $p \sim 3$ (e.g., Chevalier & Fransson 2006; Soderberg et al. 2010; Chakraborti et al. 2015). From a purely theoretical perspective, both analytical models and particle-in-cell (PIC) simulations confirm that $p = 2.2$ is expected in the cases of ultra-relativistic shocks where particle acceleration is very efficient. We thus conclude that a late onset of a weak on-axis afterglow emission is unlikely to provide a satisfactory explanation of our observations across the electromagnetic spectrum, and we consider alternative explanations below.

3.2. Constraints on Off-axis Jets

A delayed onset of the X-ray emission can originate from the presence of an off-axis jet, originally pointed away from our line of sight. For a simple model of a point source at an angle $\theta_{\rm obs}$, moving at a Lorentz factor Γ, the peak in the light curve occurs when the beaming cone widens enough to engulf the line of sight, $\Gamma(t_{\rm pk}) \sim 1/\theta_{\rm obs}$ (e.g., Granot et al. 2002). This is a purely dynamical effect that does not depend on the micropysical parameters ϵ_e and ϵ_B (which instead concur to determine the overall luminosity of the emission). From Granot & Sari (2002), the evolution of the Lorentz factor of a blast wave propagating into an ISM can be parameterized as $\Gamma(t) \sim 6.68 (E_{k,\rm iso,52}/n_0)^{1/8} t_{\rm days}^{-3/8}$, which gives $\theta_{\rm obs} \sim 0.15 (E_{k,\rm iso,52}/n_0)^{-1/8} t_{\rm pk,days}^{3/8}$ or $\theta_{\rm obs} \sim 0.2\ (E_{k,50}/n_0)^{-1/6} t_{\rm pk,days}^{1/2}$. Before peak the off-axis model predicts a steep rise, with the flux scaling $\propto t^2$. As we argued above, the mild temporal evolution of the detected X-ray emission suggests a peak not too far from our last epoch of observation at $\sim$15 days. We find $\theta_{\rm obs} \sim (15^\circ\text{–}30^\circ)(E_{k,50}/n_{-3})^{-1/6}$ deg for $t_{\rm pk} = 15\text{–}70$. If GW170817 harbored a relativistic off-axis jet with similar parameters to cosmological short GRBs ($E_k \sim 10^{49-50}$ erg and $n \sim 10^{-3}$ cm^{-3}; Fong et al. 2015), this simple analytical scaling suggests off-axis angles $\theta_{\rm obs} \sim 20^\circ\text{–}40^\circ$.

The actual values of the flux detected (and undetected) in the X-rays and radio pose additional constraints that break the model degeneracy in E_k and n as a function of ϵ_e and ϵ_B. We employ realistic simulations of relativistic jets propagating into an ISM to fully capture the effects of lateral jet spreading with time, finite jet opening angle, and transition into the non-relativistic regime. To this aim, we run the publicly available code BOXFIT (v2; van Eerten et al. 2010; van Eerten & MacFadyen 2012), varying E_k, n, p, ϵ_B, and θ_j (jet opening angle) and calculate the off-axis afterglow emission as observed from different lines of sight $\theta_{\rm obs}$, with $\theta_{\rm obs}$ varying from 5° to 90° (i.e., equatorial view). We explore a wide portion of parameter space corresponding to $E_k = 10^{48}\text{–}10^{51}$ erg, $n = 10^{-4}\text{–}1$ cm^{-3}, and $\epsilon_B = 10^{-4}\text{–}10^{-2}$. In our calculations, we assume the fiducial value $\epsilon_e = 0.1$ (e.g., Sironi et al. 2015). For each parameter set, we consider two values for the power-law index of the electron distribution

$p = 2.4$ (median value from short GRBs afterglows from Fong et al. 2015) and $p = 2.2$ (as expected from particle acceleration in the ultra-relativistic limit; Sironi et al. 2015), and we run each simulation for a collimated $\theta_j = 5^\circ$ jet and a jet with $\theta_j = 15^\circ$, representative of a less collimated outflow (Table 1). As a comparison, the measured θ_j in short GRBs range between 3° and 10 °with notable lower limits $\theta_j > 15^\circ$ and $\theta_j > 25^\circ$ for GRBs 050709 and 050724A (Fong et al. 2015 and references therein).

The results from our simulations can be summarized as follows. (i) While we find a set of solutions with $p = 2.4$ that can adequately fit the X-ray light curve, all of these simulations violate our radio limits as we detail in Alexander et al. (2017a). Models with $p \geqslant 2.4$ are ruled out, and we will not discuss these simulations further. (ii) Models that intercept the measured X-ray flux, but with $t_{\rm pk} \gg 15$ days, overpredict the radio emission, for which we have observations extending to $t \sim 40$ days (Alexander et al. 2017a). Jets with $E_k > 10^{50}$ erg belong to this category and are not favored. (iii) Most high-density environments with $n \sim 0.1$–$1\ {\rm cm}^{-3}$ cause an earlier deceleration of the jet. As a consequence, these models require $\theta_{\rm obs}$ between 40° and 60° to match the X-ray flux evolution (i.e., a range of $\theta_{\rm obs}$ not favored by the early blue colors of the kilonova; Cowperthwaite et al. 2017; Nicholl et al. 2017) and are not consistent with the radio limits. (iv) Low-energy jets with $E_k \sim 10^{48}$ erg also have shorter deceleration times and require $\theta_{\rm obs} > 45^\circ$ to explain the X-ray observations (and are consequently not favored by the kilonova colors). (v) Finally, wider jets have a larger allowed parameter space and are favored based on their broader light curves around peak time.

We identify a family of solutions that adequately reproduce the current data set across the spectrum (Figures 2–3). The successful models are characterized by an off-axis jet with $10^{49}{\rm erg} \lesssim E_k \lesssim 10^{50}$ erg, $\theta_j = 15^\circ$ viewed ∼20°–40° off-axis and propagating into an ISM with $n \sim 10^{-4}$–$10^{-2}\ {\rm cm}^{-3}$, depending on the value of $\epsilon_B = 10^{-4}$–10^{-2}. The dependency of the best-fitting $\theta_{\rm obs}$ values on n and ϵ_B is illustrated in Figure 4. The successful models are portrayed in Figures 2–3. Collimated outflows with $\theta_j = 5^\circ$ satisfy the observational constraints only for $E_k = 10^{49}$ erg, $\epsilon_B = 10^{-4}$, $n \sim 10^{-3}\ {\rm cm}^{-3}$, and $\theta_{\rm obs} \sim 16^\circ$. From Figures 2–3 it is clear that the optical emission from the off-axis afterglow (green line in the right column plots) is always negligible compared to the contemporaneous kilonova emission. It is also worth noting that these models predict a radio flux density that is close to our flux limits (purple line and points), thus providing support to our tentative VLA detection at $t \sim 20$ days at the level of ∼20 μJy (Alexander et al. 2017a). Our favored models are not in disagreement with the radio detection of a faint transient at the level of S/N = 5 previously reported by Mooley et al. (2017) and Corsi et al. (2017) ∼15 days post-merger (Hallinan et al. 2017), and are fully consistent with our radio detection at 6 GHz at $t = 39.4$ days, as detailed in Alexander et al. (2017a).

3.3. Emission from the Central Engine

Short GRBs are sometimes accompanied by late-time X-ray emission (e.g., Perley et al. 2009; Margutti et al. 2011; Fong et al. 2014), which may originate from a long-lived central engine, such as an accreting black hole (e.g., Perna et al. 2006) or a millisecond magnetar (e.g., Metzger et al. 2008).

GW170817 was accompanied by luminous optical and infrared emission, consistent with predictions for the kilonova emission originating from r-process radioactive heating of the merger ejecta (Chornock et al. 2017; Cowperthwaite et al. 2017; Nicholl et al. 2017). The observed X-ray transient is unlikely to originate from the central engine because the signal would be blocked by the photoelectric absorption in this same ejecta along the viewer's line of sight.

Given the estimated ejecta mass of $\gtrsim 10^{-2} M_\odot$ and mean velocity $v_{\rm ej} \sim 0.1$–$0.2c$ (Chornock et al. 2017; Cowperthwaite et al. 2017; Nicholl et al. 2017), the optical depth through the ejecta of radius $R \sim v_{\rm ej} t$ and density $\rho \sim M_{\rm ej}/(4\pi R^3/3)$ is approximately given by

$$\tau_{\rm X} \simeq \rho R \kappa_{\rm X} \approx 90 \left(\frac{\kappa_{\rm X}}{1000\ {\rm cm^2\ g^{-1}}}\right)\left(\frac{M_{\rm ej}}{10^{-2} M_\odot}\right)\left(\frac{v_{\rm ej}}{0.2c}\right)^{-2} \times \left(\frac{t}{2\ {\rm week}}\right)^{-2}, \quad (1)$$

where $\kappa_{\rm X} \sim 1000\ {\rm cm^2\ g^{-1}}$ is the expected bound-free opacity of neutral or singly ionized heavy r-process nuclei at X-ray energies ∼ a few keV (e.g., Metzger 2017). The fact that $\tau_X \gg 1$ suggests that any X-ray signal from the engine would be highly suppressed, by a factor $e^{-\tau_{\rm X}} \ll 1$. X-rays could escape at an earlier stage only if they were sufficiently powerful $L_X \gtrsim 10^{43}$–$10^{44}\ {\rm erg\ s^{-1}}$ to photoionize the ejecta, as is clearly not satisfied by the observed source $L_X \lesssim 10^{40}\ {\rm erg\ s^{-1}}$ (Metzger & Piro 2014).

Such a high optical depth is not necessarily expected for on-axis viewers more typical of gamma-ray bursts, especially at early times when the engine is most powerful, because the relativistic jet may clear a low-density funnel through the ejecta along the binary axis. As our orientation with GW170817 is unlikely to be so fortuitous, a central-engine origin of the X-ray emission is disfavored.

4. Summary and Conclusions

We present the first X-ray detection from a GW source thanks to *CXO* observations. These observations enabled the first discovery of *rising* X-ray emission that we interpret in the context of isotropic or collimated outflows (on-axis and off-axis) with different properties. Our results can be summarized as follows:

1. On-axis afterglow emission similar to that typically observed in cosmological short GRBs (i.e., $E_{k,\rm iso} \sim 10^{51}$ erg) is clearly ruled out.
2. A late (on-axis or isotropic) afterglow onset, due to the deceleration of a mildly relativistic outflow can explain the X-ray observations but likely violates the radio limits.
3. A central-engine origin of the X-ray emission is disfavored, as from the kilonova parameters that we infer in Cowperthwaite et al. (2017), Nicholl et al. (2017), and Chornock et al. (2017) we derive a large optical depth that would prevent the X-rays from escaping and reach the observer.
4. Current radio and X-ray observations are consistent with the emission from a relativistic jet with $\theta_j = 15^\circ$, $10^{49}\ {\rm erg} \leqslant E_k \leqslant 10^{50}$ erg, viewed ∼20°–40° off-axis and propagating into an ISM environment with

$n = 10^{-4}$–$10^{-2}\,\mathrm{cm}^{-3}$ depending on $\epsilon_B = 10^{-4}$–10^{-2}. Very collimated outflows with $\theta_j \sim 5^\circ$ are not favored by observations.

The discovery of X-ray emission from GW170817 marks a milestone in connecting on-axis GRBs with BNS mergers, and sets the stage for all future GW events with detected X-ray emission. Late-time X-ray monitoring of GW170817 at $t \geqslant 100$ days (when it will be observable again with the *CXO*) will provide additional, crucial information to solve the model degeneracies and test our predictions. Our inferences on the observing angle with respect to the jet axis might be testable using GW information from advanced LIGO/Virgo on the binary inclination, inasmuch as the accuracy of the GW measurement is comparable to ours.

Support for this work was provided by the National Aeronautics and Space Administration through *Chandra* Award Number GO7-18024X issued by the *Chandra X-ray Observatory* Center, which is operated by the Smithsonian Astrophysical Observatory for and on behalf of the National Aeronautics Space Administration under contract NAS8-03060. W.F. acknowledges support for program number *HST*-HF2-51390.001-A, provided by NASA through a grant from the Space Telescope Science Institute, which is operated by the Association of Universities for Research in Astronomy, Incorporated, under NASA contract NAS5-26555. C.G. acknowledges University of Ferrara for use of the local HPC facility co-funded by the "Large-Scale Facilities 2010" project (grant 7746/2011). Development of the Boxfit code was supported in part by NASA through grant NNX10AF62G issued through the Astrophysics Theory Program and by the NSF through grant AST-1009863. The Berger Time-Domain Group at Harvard is supported in part by the NSF through grants AST-1411763 and AST-1714498, and by NASA through grants NNX15AE50G and NNX16AC22G. D.A.B. is supported by NSF award PHY-1707954. Simulations for BOXFITv2 have been carried out in part on the computing facilities of the Computational Center for Particle and Astrophysics of the research cooperation "Excellence Cluster Universe" in Garching, Germany.

ORCID iDs

R. Margutti https://orcid.org/0000-0003-4768-7586

References

Abbott, B. P., Abbott, R., Abbott, T. D., et al. 2017, PhRvL https://doi.org/10.1103/PhysRevLett.119.161101
Alexander, K. D., Berger, E., Fong, W., et al. 2017a, ApJL, https://doi.org/10.3847/2041-8213/aa905d
Alexander, K. D., Fong, W., & Berger, E. 2017b, GCN, 21897
Allam, S., Annis, J., Berger, E., et al. 2017, GCN, 21530
Berger, E. 2014, ARA&A, 52, 43
Blanchard, P. K., Berger, E., Fong, W., et al. 2017, ApJL, https://doi.org/10.3847/2041-8213/aa9055
Blandford, R. D., & McKee, C. F. 1976, PhFl, 19, 1130
Burrows, D. N., Hill, J. E., Nousek, J. A., et al. 2005, SSRv, 120, 165
Cenko, S. B., Emery, S. W. K., Campana, S., et al. 2017, GCN, 21572
Chakraborti, S., Soderberg, A., Chomiuk, L., et al. 2015, ApJ, 805, 187
Chevalier, R. A., & Fransson, C. 2006, ApJ, 651, 381
Chornock, R., Berger, E., Kasen, D., et al. 2017, ApJL, https://doi.org/10.3847/2041-8213/aa905c
Connaughton, V., Blackburn, L., Briggs, M. S., et al. 2017, GCN, 21506
Corsi, A., Hallinan, G., Mooley, K., et al. 2017, GCN, 21815
Coulter, D. A., Kilpatrick, C. D., Siebert, M. A., et al. 2017a, Sci, https://doi.org/10.1126/science.aap9811
Coulter, D. A., Kilpatrick, C. S., Siebert, M. R., et al. 2017b, GCN, 21529
Cowperthwaite, P. S., Berger, E., Villar, V. A., et al. 2017, ApJL, https://doi.org/10.3847/2041-8213/aa8fc7
D'Avanzo, P., Salvaterra, R., Bernardini, M. G., et al. 2014, MNRAS, 442, 2342
Eichler, D., Livio, M., Piran, T., & Schramm, D. N. 1989, Natur, 340, 126
Evans, P. A., Cenko, S., Kennea, D. A., et al. 2017a, Sci, https://doi.org/10.1126/science.aap9580
Evans, P. A., Kennea, J. A., Breeveld, A. A., et al. 2017b, GCN, 21550
Fong, W., & Berger, E. 2013, ApJ, 776, 18
Fong, W., Berger, E., Margutti, R., & Zauderer, B. A. 2015, ApJ, 815, 102
Fong, W., Berger, E., Metzger, B. D., et al. 2014, ApJ, 780, 118
Fong, W., Berger, E., Blanchard, P. K., et al. 2017a, ApJL, https://doi.org/10.3847/2041-8213/aa9018
Fong, W., Margutti, R., Haggard, D., et al. 2017b, GCN, 21768
Gehrels, N., Chincarini, G., Giommi, P., et al. 2004, ApJ, 611, 1005
Goldstein, A., Veres, P., Burns, E., et al. 2017, ApJL, https://doi.org/10.3847/2041-8213/aa8f41
Granot, J., Panaitescu, A., Kumar, P., & Woosley, S. E. 2002, ApJL, 570, L61
Granot, J., & Sari, R. 2002, ApJ, 568, 820
Haggard, D., Nynka, M., Ruan, J. J., et al. 2017a, ApJL, https://doi.org/10.3847/2041-8213/aa8ede
Haggard, D., Nynka, M., Kalogera, V., Evans, P., & Cenko, B. 2017b, GCN, 21798
Hallinan, et al. 2017, Sci, https://doi.org/10.1126/science.aap9855
Kalberla, P. M. W., Burton, W. B., Hartmann, D., et al. 2005, A&A, 440, 775
LIGO Scientific Collaboration & Virgo Collaboration 2017a, GCN, 21509
Margutti, R., Chincarini, G., Granot, J., et al. 2011, MNRAS, 417, 2144
Margutti, R., Zaninoni, E., Bernardini, M. G., et al. 2013, MNRAS, 428, 729
Margutti, R., Fong, W., Berger, E., et al. 2017, GCN, 21648
Metzger, B. D. 2017, LRR, 20, 3
Metzger, B. D., & Berger, E. 2012, ApJ, 746, 48
Metzger, B. D., & Piro, A. L. 2014, MNRAS, 439, 3916
Metzger, B. D., Quataert, E., & Thompson, T. A. 2008, MNRAS, 385, 1455
Mooley, K. P., Hallinan, G., & Corsi, A. 2017, GCN, 21814
Narayan, R., Paczynski, B., & Piran, T. 1992, ApJL, 395, L83
Nicholl, M., Berger, E., Kasen, D., et al. 2017, ApJL, https://doi.org/10.3847/2041-8213/aa9029
Perley, D. A., Metzger, B. D., Granot, J., et al. 2009, ApJ, 696, 1871
Perna, R., Armitage, P. J., & Zhang, B. 2006, ApJL, 636, L29
Piran, T. 2004, RvMP, 76, 1143
Rybicki, G. B., & Lightman, A. P. 1979, Radiative Processes in Astrophysics (New York: Wiley-Interscience)
Sari, R., & Piran, T. 1999, ApJ, 520, 641
Savchenko, V., Mereghetti, S., Ferrigno, C., et al. 2017, GCN, 21507
Schutz, B. F. 2011, CQGra, 28, 125023
Sekiguchi, Y., Kiuchi, K., Kyutoku, K., Shibata, M., & Taniguchi, K. 2016, PhRvD, 93, 124046
Sironi, L., Keshet, U., & Lemoine, M. 2015, SSRv, 191, 519
Soares-Santos, M., Holz, D., Annis, J., et al. 2017, ApJL, https://doi.org/10.3847/2041-8213/aa9059
Soderberg, A. M., Chakraborti, S., Pignata, G., et al. 2010, Natur, 463, 513
Troja, E., Piro, L., Sakamoto, T., Cenko, S. B., & Lien, A. 2017a, GCN, 21765
Troja, E., Piro, L., van Eerten, H. J., et al. 2017b, Natur, https://doi.org/10.1038/nature24290
Valenti, S., Sand, D. J., Yang, S., et al. 2017, ApJL, https://doi.org/10.3847/2041-8213/aa8edf
van Eerten, H., Zhang, W., & MacFadyen, A. 2010, ApJ, 722, 235
van Eerten, H. J., & MacFadyen, A. I. 2012, ApJ, 751, 155
Yang, S., Valenti, S., Sand, D., et al. 2017, GCN, 21531